Transactions of the 17th International Conference on Structural Mechanics in Reactor Technology (SMiRT 17)
Prague, Czech Republic, August 17 –22, 2003

Paper # WG01-2

Influence of Silica on Stress Corrosion Cracking of Alloy 600 and Alloy 690

H.P. Kim, S. H. Uhm, Y. M. Nho, D. J. Kim, Y. S. Lim, S.S. Hwang, J.S. Kim

Korea Atomic Energy Research Institute, P.O. Box 105, Yusong, Taejon, Korea 305-600

ABSTRACT

Silicate is a major constituent of sludge on the tubesheet region of PWR steam generators, where stress corrosion cracking (SCC) of the steam generator tubing generally occurs in nuclear power plants. In this work, the effects of silicate on SCC of Alloy 600 and Alloy 690 have been studied in 10 % NaOH and 40 % NaOH with and without 2 g/l SiO_2 at 315℃. The experiments were performed using C-ring specimens at 200 mV above the corrosion potential. The stress at the apex of the C-ring specimen ranged from about 300 MPa to about 600 MPa. Polarization behaviors of Alloy 600 and Alloy 690 were also studied. High temperature mill annealed Alloy 600, sensitized Alloy 600, thermally treated Alloy 600 and thermally treated Alloy 690 were used for the SCC and polarization test. Composition profiles of the deposit layer on Alloy 600 and Alloy 690 were examined with an Auger electron microscope. The degree of sensitization was evaluated with a modified Huey test and TEM-EDX. Effects of silica on SCC of Alloy 600 and Alloy 690 are discussed in terms of polarization behavior and the oxide layer composition.

Key Words: stress corrosion cracking, Alloy 600, Alloy 690, polarization curves, AES, TEM, NaOH, silica.

INTRODUCTION

Secondary side stress corrosion cracking (SCC) of a steam generator tube in pressurized water reactor has been a great concern in recent years. Because the SCC has occurred predominantly below the deposit on top of the tube sheet, the deposit and crevice chemistry in the deposit have been studied extensively [1-4]. These studies have established that a copper compound in the deposit elevates the corrosion potential of the tube [5] and accelerates pitting under the concurrent action of a chloride ion [6] and that lead in the deposit accelerates SCC [7]. However, the role of silicon compound which has been found abundantly in the deposit is still unclear in the SCC process.

Beneficial effects of silicon compound on SCC were proposed based on observation that some plant with a higher silica content in the blow down water have experienced less secondary SCC [8] and the presence of silicon compound in a caustic solution improved SCC resistance [9]. On the contrary, harmful effects of silicon compound on SCC were proposed based on findings that a deposit having an alumino-silicate gel sublayer associated with an organic compound were found on degraded tubes in nuclear power plants and the sublayer induced the formation of a non-protective, thin brittle layer at the interface of alloy [10]. The fore mentioned controversy about the role of silicon compound implies that it is very difficult to pin point the specific compound having an influence on SCC because the

deposit on the top of tube sheet is rather complex in composition and structure.

The purpose of the work is to establish the role of silica on SCC initiation and propagation of Alloy 600 and Alloy 690 in a caustic solution.

EXPERIMENTAL PROCEDURE

Alloy designations and their chemical compositions are shown in Table 1. First two letters, HT, SN and TT in alloy designation mean high temperature mill annealed, sensitized and thermally treated alloys, respectively. Three digits, 600 and 690 in alloy designation mean Alloy 600 and Alloy 690, respectively. Last letter in the alloy designation stands for heat. As received materials were nuclear grade HT600 and TT690. SN600 and TT600 were prepared by heat treating the as-received HT600 at 600^{o}C for 24 Hrs and 715 ^{o}C for 15 Hrs, respectively. Some of the tubing was elongated by 20 % to increase yield strength and thereby apply a higher stress at the apex of the C-ring specimen

Cr depletion around the grain boundary was examined with JEOL-2000 FXII (operating voltage 200kV) equipped with an Oxford Link (Model ISIS-5947) EDX spectrometer. Cr depletion around the grain boundary was also measured with a modified Huey test under the condition of exposure of heat treated Alloy 600 in boiling 25 % HNO_3 for 48 Hrs.

All test solutions were prepared by adding reagent grade chemicals to demineralized water. Solutions for polarization and SCC test were deoxygenated 10 % NaOH and 40 % NaOH with or without 2g/l SiO_2. SCC tests were performed at 315^{o}C using C-ring specimens at corrosion potential at 200 mV above the corrosion potential in 10 % NaOH and 40 % NaOH with or without 2g/l SiO_2. Polarization curves were obtained at 315^{o}C by scanning from -1.5V vs open circuit potential (OCP) to 1.5V vs OCP at a scan rate of 1mV/sec. In-depth composition profiles of the films on the C-ring specimen were obtained with Auger electron spectroscopy (AES), Physical Electronics PHI Model 680, by sequentially sputtering by Argon ion bombardment and performing an Auger analysis. Sputtering rate was 300 A/min on SiO_2 for the film on a free surface and 200A/min on SiO_2 for the film on a SCC fracture surface.

RESULT

Cr Depletion around the Grain Boundary

Cr depletion profiles across the grain boundaries were measured with TEM. The spacing between the edge of the intergranular carbide and the edge of the EDX beam was about 60 nm to avoid the EDX beam passing through the intergranular carbide by beam broadening. Minimum Cr concentration in the grain boundary was about 13.2 wt. % for HT600A, 7.3 wt. % for SN600A and 10.5 wt. % for TT600A. Full width at a half of the maximum (FWHM) is about 270 nm for HT600A, 300 nm for SN600A and 360 nm for TT600A.

Weight loss was measured with the Modified Huey test. HT600A showed a slight weight loss of about 115×10^{-9} Kg/m^2/sec because it was cooled relatively fast from the mill anneal temperature to room temperature to precipitate intergranular carbide. SN600A was completely disintegrated because of extensive precipitation of intergranular carbide and

concurrent Cr depletion around the grain boundary. TT600A showed much less weight loss of about $22x10^{-9}$ $Kg/m^2/sec$ compared to SN 600A because the heat treatment temperature was high enough for Cr diffusion from the matrix back to the Cr depleted grain boundary.

SCC

Average SCC crack propagation rates in 10% NaOH and 40 % NaOH with and without 2 g/l SiO_2 are shown in Table 2. The SCC resistance of Alloy 600 increased in the following order in 10 % and 40 % NaOH solutions with and without 2g/l SiO2: HT Alloy 600, SN Alloy 600 and TT Alloy 600. Both HT600A and SN600A stressed to 600 MPa were through wall cracked and TT600A stressed to 600 MPa was almost through wall cracked in 10% NaOH in 10 days. On the other hand, HT600A stressed to 600 MPa was partially cracked and both SN600A and TT600A stressed to 600 MPa were not cracked in 10 % NaOH with 2g/l SiO_2 in 10days. The above mentioned results imply that silicate added to 10% NaOH would retard SCC of Alloy 600. Table 2 shows that the presence of silica in 40% NaOH also increased SCC resistance of HT600A as in 10% NaOH, however it decreased the SCC resistance of SN600A and TT600A. SCC resistance of Alloy 600 decreased as the NaOH concentration increased from 10% NaOH to 40% NaOH. Alloy 690 was not cracked during given the test period in 10% NaOH and 40% NaOH with or without 2 g/l SiO_2.

Polarization Curve

Polarization curves are shown in Fig. 1. The shape of the polarization curve highly depends on preconditioning and scan rate. However, polarization curves obtained at the same preconditioning and scan rate will not coincide with each other. This may be attributed to the following factors: Spacing between the working electrode and reference electrode was not precisely controlled; IR drop contribution to the potential was not same. Therefore, in this work, 5 polarization curves obtained for each condition were obtained and the typical one for each condition is presented. The work showed that the presence of silica decreased current density and changed the shape of the polarization curves of Alloy 600 and Alloy 690 above the corrosion potential in 10% NaOH. However, the presence of silica has a slight effect on the polarization curves of Alloy 600 and Alloy 690 above the corrosion potential in 40% NaOH. Passivation current densities of Alloy 600 and Alloy 690 showed dramatic increase as a function of NaOH concentration in the range of 10% to 40%.

AES in-depth Composition Profile

AES in-depth composition profile was obtained on the free surface, SCC fracture surface near the SCC crack initiation site and the SCC fracture surface near the SCC crack tip of the C-ring specimen. AES depth profile including oxygen and carbon did not show clear a trend of composition variation with depth of the corrosion product. Therefore, depth profile of the atomic fractions ($xi/\sum xi$) of major alloying elements in 10%NaOH with and without 2g/l SiO_2 are plotted in Fig. 2. Both Ni enrichment and Cr depletion in the outermost layer of the corrosion product compared to the Alloy 600 composition was clearly found in the location from free surface to crack tip in 10% NaOH. On the other hand, Ni depletion and Cr enrichment in the outermost layer of corrosion product were found in the location from free surface to crack initiation site in 10% NaOH with 2g/l SiO_2. However, Ni depletion and Cr enrichment in the outermost layer of the

corrosion product was not found in the crack tip in 10% NaOH with 2g/l SiO_2. Atomic fraction of major alloying elements in the corrosion product approached alloy composition as the corrosion product was sputtered away. Silicon content which was incorporated into the outer layer of the corrosion product decreased with the depth of the corrosion product (Fig.3).

DISCUSSION

Cr Depletion around Grain Boundary

Minimum Cr concentration at the grain boundary measured by TEM and the modified Huey test results indicate that HT 600 is slightly sensitized, SN 600 is heavily sensitized and that TT 600 is partially healed by Cr back diffusion into the grain boundary but has a wider Cr depletion width compared to SN 600. Thermodynamic and Kinetic models [11, 12] derived on the basis of local equilibrium between carbon and chromium at the grain boundary suggest that chromium concentration at the grain boundary is minimal at the beginning of chromium carbide precipitation and then increases with heat treatment time at a given temperature and heat treatment temperature and that chromium depletion around the grain boundary increases with heat treatment time at a given temperature and heat treatment temperature. The minimum chromium concentration of about 13.2 wt. % for HT 600 and 7.3 wt. % for SN600 do not coincide with the trend predicted from the thermodynamic and kinetic models [11, 12]. The models predict higher Cr concentration at the grain boundary of HT600 than that of SN600 because the bulk carbon concentration is higher in HT600 than in SN600. The discrepancy may be attributed to the high beam diameter of 20-40nm used in TEM work and measurement of Cr depletion at the midpoint between the two intergranular carbides in the grain boundary. The best match of composition profile of the thermodynamic and kinetic model with that of the TEM measurement across the grain boundary could be achieved by measuring the composition with a small beam diameter at a point nearest to the intergranular carbide and by avoiding the beam passing through the intergranular carbide. The full width at a half of the maximum for chromium depletion of about 270nm for HT 600 and 300nm for SN600 and 360nm for TT600 coincide with the trend predicted by the thermodynamic and kinetic models.

SCC

The increase in SCC resistance of Alloy 600, with an order from HT600, SN600 to TT600, in 10 % and 40 % NaOH solutions is also valid for 10 % and 40 % NaOH solutions with 2g/l SiO_2. This is consistent with our previous work [13] that the increase in SCC resistance, with an order from HT600, SN600 to TT600, in a caustic solution is contributed to the dominance of the beneficial effect of intergranular carbide over the harmful effect of chromium depletion around the grain boundary in intergranular SCC.

Enhanced SCC resistance of Alloy 600 in 10% NaOH with silica compared to that in pure 10% NaOH indicates that silica or silicate significantly effects SCC in a caustic solution. The higher SCC resistance of Alloy 600 in 10 % NaOH with 2 g/l SiO_2 is possibly attributed to the lower current density above the corrosion potential in the polarization curves (Fig. 1), higher Cr fraction in the outermost layer of the corrosion product on the free surface and crack initiation site of specimen (Fig. 2) and incorporation of silicon into the outer layer of the corrosion product (Fig. 3) under the presence of

SiO_2 in 10 % NaOH. Degree of chromium enrichment in outermost layer on the free surface and crack initiation site in 10%NaOH with 2g/l SiO2 obtained in this work is more significant than that observed by Navas, et al. [9], even though the silica content in this work is less than that used by them. On the contrary, the presence of silica almost has no effect on Cr fraction in the outermost layer of the corrosion product near the crack tip, suggesting that silica or its dissolved ion has difficulty in migrating from the bulk solution to the crack tip. These results imply that a higher Cr fraction in the outermost layer of the corrosion product and/or incorporation of silicon into outer layer of the corrosion product would increase the stability of the corrosion product, consequently reducing current density in the polarization curves and manifesting in the enhancement of SCC resistance especially in SCC initiation and early crack propagation stage. Augmented SCC resistance of Alloy 600 in 10% NaOH with silica compared to that in pure 10% NaOH is compatible with studies involving the addition of silica or silicate to a caustic solution [8] and incorporating the correlation between secondary water chemistry and steam generator tube degradation trend [9]. This work emphasizes and establishes that silica in 10 % NaOH reduces crack initiation and early crack propagation but seems to have little effect on later crack propagation based on the composition profile of the deposit. However, based on deposit analysis of pulled tubes from nuclear power plants, Sala, et al., [10] suggested that silicate is detrimental to SCC. They concluded this from the observation that deposits having an alumino-silicate gel sublayer associated with an organic compound on degraded tubes induced the formation of a non-protective, thin brittle layer. Deposits on specimens in laboratory tests such as adding silica or silicate to a caustic solution is relatively simple compared to that on pulled tubes from nuclear power plants. The suggestion that the presence of silicate in secondary water is beneficial to SCC is not consistent with the observation that alumino-silicate deposit on a tube is harmful to SCC. At this stage even though our work as well as other work performed in the laboratory strongly suggests that silica or silicate is beneficial to SCC. However, the addition of silica or silicate to secondary water should be considered cautiously because the beneficial effect requires additional validation in a complex environment such as the deposit on the tubesheet in a nuclear power plant.

Beneficial effect of silica on SCC resistance of Alloy 600 in 40% NaOH could not be validated in this work because HT600 and SN600 seem to be more resistant to SCC, whereas, TT600 is more susceptible to SCC in the presence of 2g/l SiO_2 in 40 % NaOH. Moreover, the presence of silicate in 40%NaOH has little effect on the current density of the polarization curves.

CONCLUSION

1. Presence of silica enhanced SCC resistance of Alloy 600 and reduced the current density of the polarization curve above the corrosion potential in 10% NaOH while it has little effect on SCC and the current density of the polarization curve above the corrosion potential in 40% NaOH.
2. Presence of silica caused Cr enrichment in the outermost layer of the corrosion product on the free surface and crack initiation site. However, it had no effect on the composition profile of the corrosion product on the crack tip, indicating that migration of the silicon compound to the crack tip is limited. Silicon was found to be incorporated into the outer layer of the corrosion product.

3. Cr enrichment in the outermost layer of the corrosion product and/or incorporation of silicon into the outer layer of the corrosion product under the presence of silica in 10% NaOH seem to increase the stability of the corrosion product and thereby enhancing SCC initiation at the early propagation stage.

ACKNOWEDGEMENT

This work has been done as a part of the Steam Generator Project of the Mid and Long-Term Program financially supported by the MOST in Korea.

REFERECCES

1. Lancha, A.M., Gomez-Briceno, D., Garcia, M. and Toribio, E. L, "AES and SEM/EDS Analysis of Deposits in Pulled Steam Generator Tubes", Sixth Intern. Symp. on Environmental Degradation of Nuclear Power Systems, pp. 89-95, California August, 1993.
2. Vaillant, F, Bousier, E, Moleiro, E and Stutzman, A., "Duplication in Laboratory of Deposits, Films and IGSCC Damage Observed on Pulled Steam Generator Tubes", Tenth Intern. Symp. on Environmental Degradation of Nuclear Power Systems, pp. 215-226, Nevada August, 2001.
3. Aaltonen, P., Makela, K. and Buddas, T., "Characterization of Oxide Scales from Loviisa Units 1 and 2", Seventh Intern. Symp. on Environmental Degradation of Nuclear Power Systems, pp. 151-162, Colorado August, 1995.
4. Saario, T. and Paine, J., "Effect of the Surface film Electric Resistance on Eddy Current Detectibility on Surface Cracks in Alloy 600 Tubes", Seventh Intern. Symp. on Environmental Degradation of Nuclear Power Systems, pp. 327-337, Colorado August, 1995.
5. Kim, U. C., "Failure Analysis of Kori Unit 1 Steam Generator Tubes", KAERI, Taejon, 1989.
6. Kim, U. C., "Failure Analysis of Kori Unit 1 Steam Generator Tubes", KAERI, Taejon, 1991.
7. Kim, U. C., "Failure Analysis of Kori Unit 2 Steam Generator Tubes", KAERI, Taejon, 1990.
8. Baum, A. J., Prabhu, P. J., Rootham, M and Zupetic, N. L., "Development of Improved PWR Secondary Water Chemistry Guidelines", Eighth Intern. Symp. on Environmental Degradation of Nuclear Power Systems, pp. 74-79, Florida August, 1995.
9. Navas, M., Gomez-Briceno, D., Garcia, M. and McIlree, A. R., "The Inhibiting Effect of Silicon Compounds on Caustic SCC of Alloy 600 MA", Proceedings of the Intern., Symp. Fontevraud IV, pp. 417-427, France 1997.
10. Sala, B., Combrade, P., Erre, R., Gelpi, A., "Local Chemistry and Formation of Deposits on the Secondary Side of Steam Generators", Sixth Intern. Symp. on Environmental Degradation of Nuclear Power Systems, pp. 215-226, California August, 1993
11. Strawstrom, A and Hillert, M., "An Improved Depleted Zone Theory of Intergranular Corrosion of 18-8 Stainless Steel", J. of the Iron and Steel Institute, Vol. 207, 1969, pp. 77-85.
12. Was, G. S. and Krugger, R. M., "A Thermodynaic and Kinetic Basis for Understanding Chromium Depletion in Ni-Cr-Fe

Alloys", Acta Metall., Vol. 55, 1985, pp. 841-854.

13. Kim, H. P., Hwang, S. S., Lim, Y. S., Kuk, I. H. and Kim, J.S., "Effect of Heat Treatment and Chemical Composition on Caustic Stress Corrosion Cracking of Alloy 600 and Alloy 690", Key Engineering Materials, Vol. 183-187, 2000, pp. 707-712.

Table 1 Alloy designation and chemical composition of steam generator tubings.

Designation	Ni	Cr	Fe	C	S	P	B	N	Si	Cu	Al	Ti
HT 600A	72.5	16.85	9.00	0.025	0.003	0.008	0.001	0.016	0.31	0.01	0.015	0.28
HT 600B	74.76	15.63	8.62	0.025	<0.001	0.007	0.004	0.01	0.14	0.03	0.21	0.34
TT 690C	58.9	29.57	10.54	0.02	0.001	0.009	0.004	0.017	0.22	0.01	0.019	0.26

Table 2 Average SCC crack propagation rate in 10% and 40% NaOH with and without 2g/l SiO_2.

Designation	Initial Stress at the Apex of C-ring(Mpa)	Average Crack Propagation Rate(mm/sec)			
		10% NaOH	10% NaOH + 2g/l SiO_2	40% NaOH	40% NaOH + 2g/l SiO_2
HT 600A	300			No SCC	
	375		No SCC	1.62×10^{-5}	No SCC
	450		8.10×10^{-7}	$>3.24 \times 10^{-4}$	
	600	$>8.10 \times 10^{-6}$	2.43×10^{-6}	$>3.24 \times 10^{-4}$	2.43×10^{-4}
HT 600B	300			$>3.24 \times 10^{-4}$	
	375			9.72×10^{-5}	2.43×10^{-4}
	450	4.05×10^{-6}	3.24×10^{-6}	$>3.24 \times 10^{-4}$	
	600	6.08×10^{-6}	$>8.10 \times 10^{-6}$	2.43×10^{-4}	$>3.24 \times 10^{-4}$
SN 600A	375		No SCC	No SCC	No SCC
	450			1.30×10^{-4}	
	600	$>8.10 \times 10^{-6}$	No SCC	$>3.24 \times 10^{-4}$	3.24×10^{-5}
TT 600A	375			No SCC	No SCC
	450		No SCC	No SCC	
	600	$>8.10 \times 10^{-6}$	No SCC	3.24×10^{-5}	2.92×10^{-4}

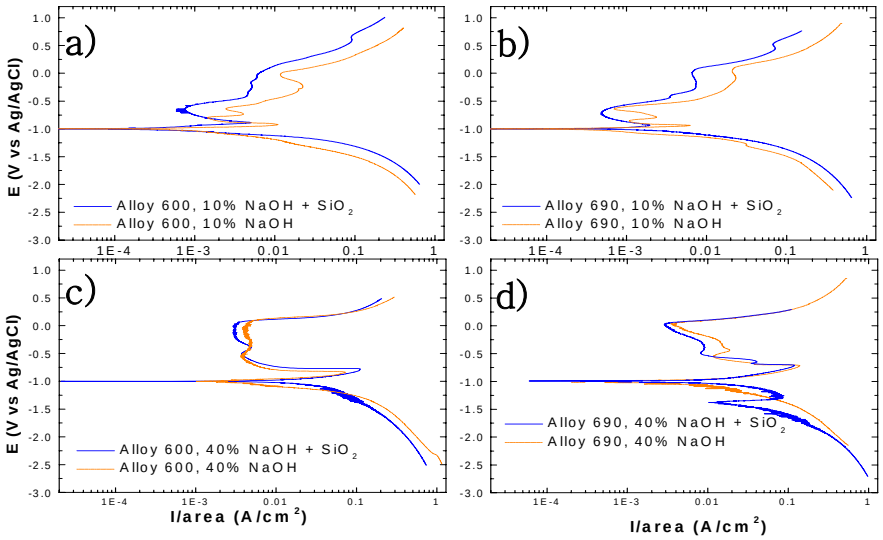

Fig. 1 Polarization curves of Alloy 600 and Alloy 690.

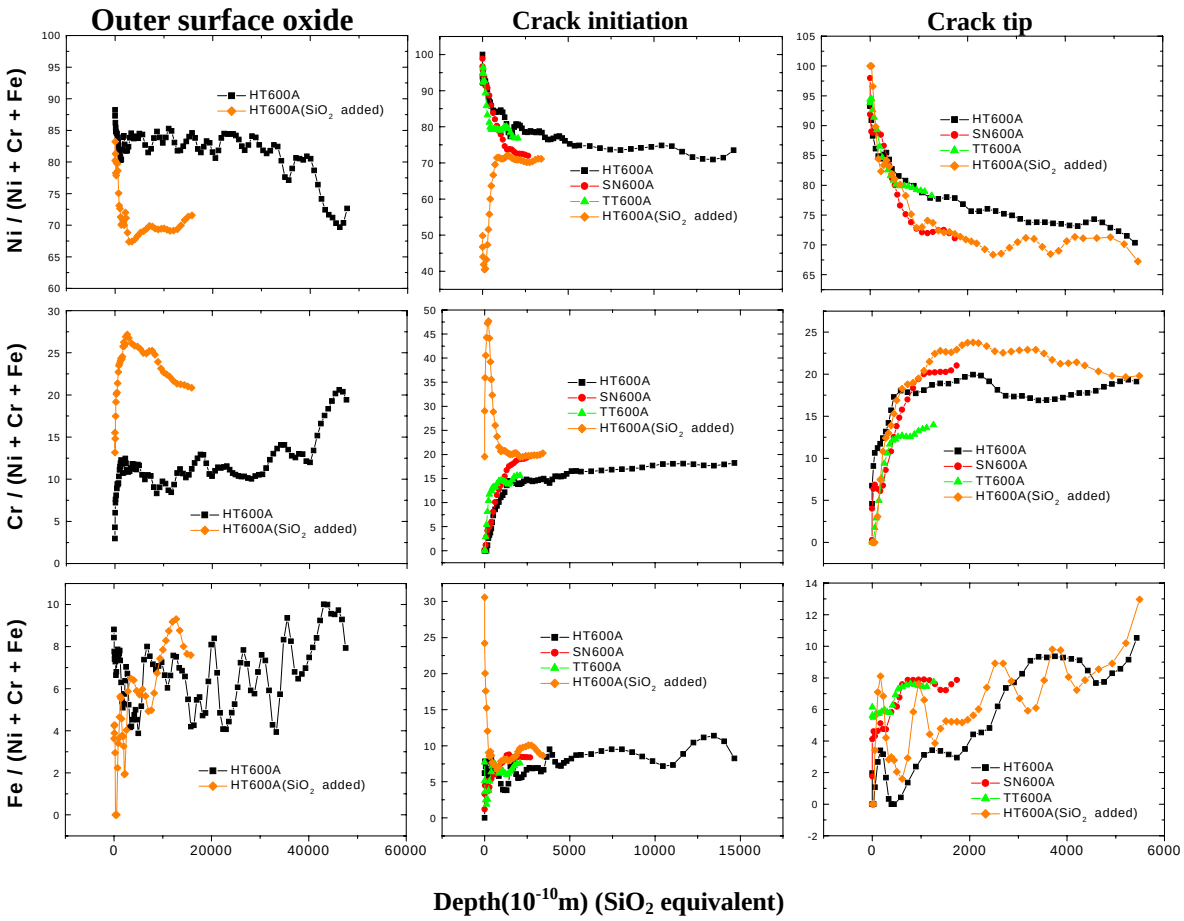

Fig.2 AES in depth atomic fraction profile of major alloying elements in a deposit.

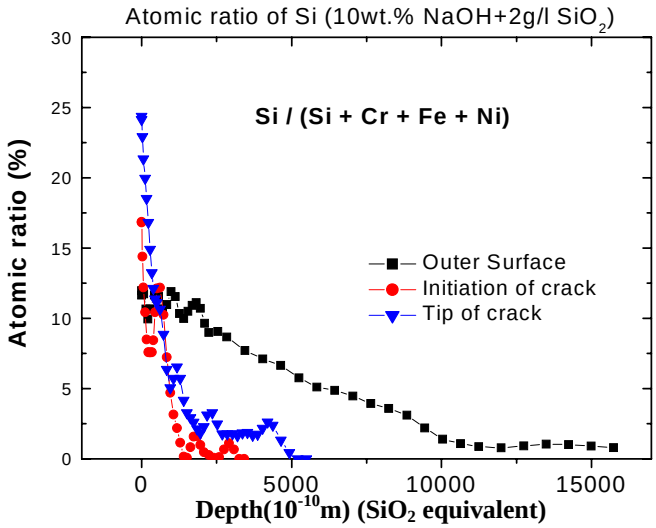

Fig.3 AES in depth Si fraction profile in a deposit.